ELSEVIER

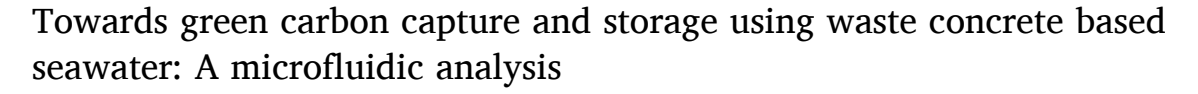
Contents lists available at ScienceDirect

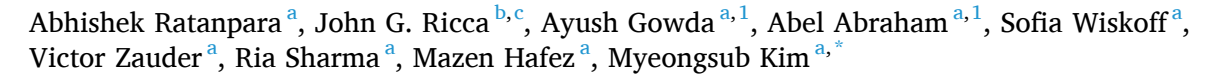
Journal of Environmental Management

journal homepage: www.elsevier.com/locate/jenvman



Research article





- ^a Department of Ocean and Mechanical Engineering, Florida Atlantic University, Boca Raton, FL, 33431, USA
- ^b Department of Chemistry and Biochemistry, Florida Atlantic University, Boca Raton, FL, 33431, USA
- ^c Center for Environmental Studies, Florida Atlantic University, Davie, FL, 33314, USA

ARTICLE INFO

Handling Editor: Jason Michael Evans

Keywords:
Carbon capture and storage
Seawater
Waste concrete
CO₂ dissolution
Microfluidics fluorescein

ABSTRACT

Carbon capture and utilization technology is the research stream dedicated to mitigating the pressing effect of rising atmospheric carbon dioxide (CO₂). The present study investigates a potential environmentally conscious solvent to capture and utilize CO_2 using waste concrete and seawater under reactor conditions. Although seawater's CO_2 soubility is low due to salinity, waste concrete raises seawater's pH and alkalinity, acting as a feedstock for CO_2 dissolution and offsetting the adverse effects of salinity. To evaluate the performance of the novel natural seawater-concrete solutions for CO_2 capture, time-dependent pH changes of solutions exposed to CO_2 were measured in a microchannel using fluorescence microscopy. The concentration of dissolved CO_2 in the solution was derived from pH change, revealing a 4-fold increase in the total dissolved carbon from 0.034 to 0.13 M and a 57.54% increase in the CO_2 dissolution coefficient from 530 to 835 μ m²/s in seawater upon concrete addition. Electrolysis further enhanced the CO_2 capture capacity of the seawater-concrete solution by increasing the pH, enabling the solid precipitation of carbonate minerals. Raman spectroscopy and scanning electron microscopy showed that electrolysis-driven precipitates are mainly amorphous calcium carbonates, useful building blocks for seashells and coral reefs.

1. Introduction

Over the past several decades, excessive anthropogenic CO₂ production and emission have led to numerous environmental and societal repercussions. The atmospheric CO₂ concentration has grown from 280 to 416 ppm since the beginning of the industrial revolution, delineating the drastic influx over recent years (Nayak et al., 2022). The increased CO₂ concentration has led to elevated global temperatures, warming the earth significantly, and subsequently bringing catastrophic natural disasters and exaggerated climatic phenomena, such as increased frequency and intensity of hurricanes (A Pielkejr et al., 2005). The melting of polar ice induced by global warming is another threatening issue raising sea levels and decreasing ocean salinity (Sabine et al., 2004). These processes have led to an alarming rate of coral bleaching,the loss of color in coral reefs. It is estimated that over 450 million people across more than 100 countries rely on coral reefs for their livelihoods, and they generate an estimated \$375 billion per year through the goods and

services they provide (Ritchie et al., 2022).

Using carbon capture and storage technology (CCS), CO2 gas can be captured from emission sources like coal power plants and stored in a safe and permanent manner. For example, anthropogenic carbon storage has reached 40 megatons per year as of 2020 with CCS technology (Ma et al., 2022). Various CCS technologies have been proposed over the decades to further improve operational efficiency and reduce associated costs. Currently, amine scrubbing for CO2 capture and injection into saline aquifers for CO_2 storage, are the most prominent methods used in real-world applications (Lv et al., 2015; Bennaceur et al., 2004). However, these available CCS methods have numerous shortcomings. Industrial amine scrubbing requires a 15-30% (v/v) monoethanolamine (MEA) solution in freshwater for CO₂ absorption, invoking a significant demand for freshwater. For example, the amine scrubbing process increases the freshwater consumption of an industrial plant by an additional 38% (Magneschi et al., 2017). Amine scrubbing also requires the regeneration of MEA at temperatures of 120-150 °C, increasing the

E-mail address: kimm@fau.edu (M. Kim).

^{*} Corresponding author.

¹ These authors contribute equally.

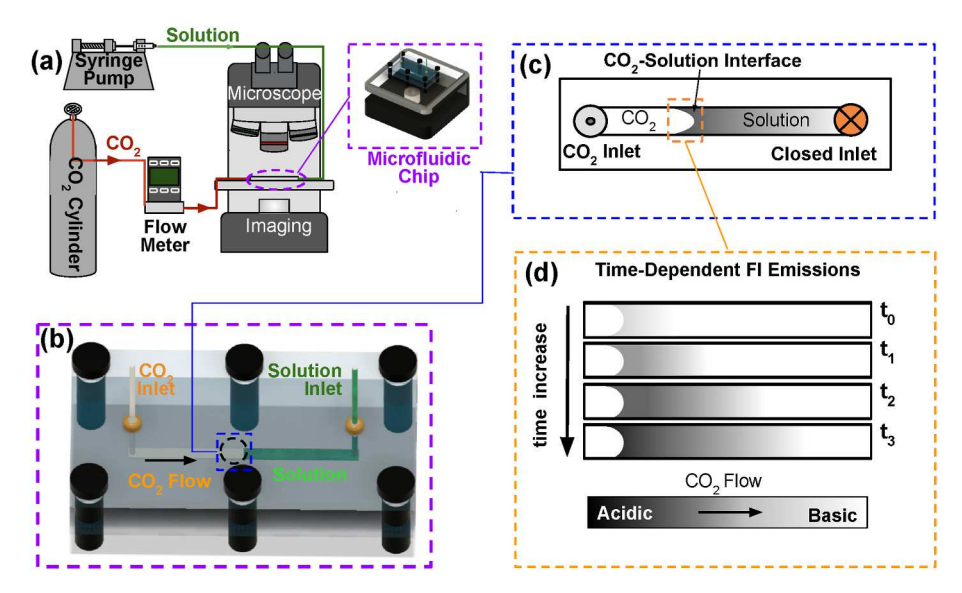


Fig. 1. (a) Schematic diagram of the experimental setup containing a microscope, a microfluidic chip, a syringe pump, and a CO₂ cylinder. (b) Aerial view of the microfluidic chip, clamped by two PMMA pieces with 6 screws. (c) Illustration showing the interface between CO₂ gas and test solution in the microchannel after injection. (d) Time-dependent pH change (gradual color variation) of the test solution in a microchannel due to CO₂ diffusion.

energy demands (Jung et al., 2013). On the other hand, once CO_2 is injected into geologic formations such as saline aquifers, CO_2 must be converted into a safe form to prevent possible environmental risks such as leakage. However, the high salinity of these formations hampers CO_2 reactions with the surrounding fluid, leading to prolonged reaction times (Ringrose et al., 2021).

More sustainable practices have been proposed in the literature to overcome the shortcomings of the conventional CCS methods. We found that natural seawater could replace freshwater in an amine-scrubbing $\rm CO_2$ capture process (Ratanpara et al., 2020). The seawater-based MEA solution yielded similar $\rm CO_2$ absorption performance to that of the DI water-based MEA solution. Furthermore, nickel nanoparticles as catalysts could further improve $\rm CO_2$ absorption in seawater (Ratanpara et al., 2021). While this approach would save ample amounts of freshwater, the issues of toxic amine solvents and energy-intensive regeneration processes persist.

To move towards CO₂ capture processes independent of the harmful chemical MEA, we investigated the role of alkaline metal ions in the capture process. Indeed, researchers have utilized industrial wastes containing alkaline earth metal ions, such as calcium (Ca²⁺) and magnesium (Mg²⁺) ions, for CO₂ capture and storage in freshwater (Botha and Strydom, 2001 Skocek et al., 2020). For example, integration of carbon sequestration into the curing process of concrete shows great potential (Kazemian and Shafei, 2023). While this process shows promise as a carbon storage option, the capture of the CO2 gas remains unanswered. Similarly, many other industrial wastes haven't been studied under reactor or reactor-simulating conditions, but their potential has been demonstrated (Baena-Moreno et al., 2022). Alkaline hydroxides increase pH, which increases CO₂ solubility, and the alkaline metal ions form ionic bonds with dissolved carbonate ions precipitating into carbonate minerals (i.e., CaCO₃ and MgCO₃). Other waste products, such as fly ash, steel slag, and concrete waste, also contain ample Ca²⁺ or Mg²⁺ ions. Concrete is considered one of the most abundant materials in the world (Gagg, 2014). Therefore, this seemingly useless industrial waste may prove to be a viable feedstock for sustainable CO_2 capture.

In this study, we analyze the effects of concrete in natural seawater for CO_2 capture and storage under reactor-like conditions (i.e., high CO_2 concentrations). The CO_2 solubility in natural seawater is inherently lower than in freshwater due to its salinity. However, with the addition of alkaline minerals from concrete, seawater can be effective for CO_2 capture. Also, with an innate abundance of alkaline ions, seawater-

concrete solutions show great potential for enhanced CO_2 storage. To evaluate the CO_2 capture performance of the seawater-concrete solution, CO_2 solubility, and the dissolution rate were measured in a microfluidic environment, and comparisons were made between natural seawater and deionized (DI) water-based solutions. The potential for CO_2 storage using seawater-concrete solution was also analyzed through electrolytic experiments, and the precipitated carbonates were examined. This study shows potential of implementing the environmentally benign concrete-based seawater solution in industrial CO_2 capture facilities.

2. Materials and methods

2.1. Materials

The microfluidic channel was fabricated from 1.5 mm thick PMMA sheets (McMaster-Carr). Uranine acid vellow 73, a pH-sensitive dye (FL116, fluorescein), was used to measure the instant pH change during the experiments. Natural seawater was collected from the Atlantic Ocean near the shore of Boca Raton, FL. The salinity of the seawater was measured by a salinity tester (HI98319, Hanna Instruments) and found to be 34.3 g/L. The concrete mix was purchased from Quikrete Holdings Incorporation. The Eclipse TE2000-S microscope was set up with a UV light source to conduct optical and fluorescence microscopy, equipped with a high-speed microscope camera (IL5, FASTEC) for recording (Fig. 1a). Pure CO₂ (99%, research grade, Airgas) was used in all experiments at constant pressure, controlled and measured by a pressure controller (185756, Alicat Scientific). Test solutions were injected into the microfluidic channel with a syringe pump (Pump 11 Pico Plus Elite, Harvard Apparatus) to ensure a constant flowrate. For the electrolysis, a BK precision 9131B triple output programmable DC power supply was utilized to regulate the voltage, and a Hanna edge portable pH probe was utilized to take pH measurements with ± 0.01 pH accuracy.

2.2. Microfluidic channels and test solutions

To fabricate microfluidic channels, PMMA sheets were cut by a $\rm CO_2$ laser cutter after being modeled in AutoCAD. The cut pieces were thermally bonded with a solution of 70% isopropyl alcohol and 30% ethanol at 50 °C for 30 min. Due to low temperature bonding, the channel shape was intact after the bonding (Nayak et al., 2010). The

straight microfluidic channel was 80,000 μ m long with a 1500 \times 1500 μ m² rectangular cross-section, having one inlet and one outlet port (Fig. 1b). A special nanoport fitting (N-333, Idex Corp.) was used to ensure the effective injection of solutions and CO₂ gas. To minimize the leakage of solutions, the microfluidic chip was clamped with two PMMA pieces (top and bottom) and 6 screws (Fig. 1b).

Four test solutions were prepared for experiments to evaluate CO₂ dissolution: DI water, DI water with 10 g/L concrete powder (DI waterconcrete), seawater, and seawater with 10 g/L concrete powder (seawater-concrete). DI water and seawater were used as control solutions compared with their concrete counterparts. From elemental analysis by microwave plasma optical emission spectroscopy (MP-OES), we found that a 50 g/L concentration of concrete induced 44% more calcium ions present in a solution after filtration than at 10 g/L concrete, and negligible pH differences were observed. Along with calcium, other elements in different solutions were also analyzed with MP-OES (Supporting Information). Therefore, a 10 g/L concentration of concrete was chosen in both DI water and seawater, as our observations showed that greater concentrations of concrete were less effective in increasing solution alkalinity and pH with respect to the amount of concrete added. It should be noted that alkalinity change with respect to the amount of concrete added will vary depending on the source of concrete (i.e., waste-concretes, in-situ concretes, etc.). Water-concrete solutions were mixed for 15 min with a magnetic stirrer and then filtered through 2.5 µm pore-size filter paper to remove undissolved particles. pH-sensitive fluorescein in a concentration of 200 µM was then added to each test solution. Due to the photosensitivity of fluorescein, all the experiments were conducted in a room with minimal light to minimize the photobleaching effect.

2.3. Fluorescence microscopy for CO2 dissolution

CO2 dissolution lowers the pH of the solutions resulting in a change in fluorescein intensity. We used the fluorescein's emission intensity at a given time and distance within the microchannel to determine the solution pH (see the Results and discussion section for details). First, the microchannel was placed under the microscope for fluid and gas injection. The volume of the test solution in the microchannel was controlled at 90 µL for consistency. Once injected, the solution inlet was closed, followed by CO2 gas injection on the other inlet port at a constant 0.5 PSIG. Throughout the experiment, the solution was kept static. As soon as the interface between CO₂ gas and the test solution was formed, the changes in emission intensities from fluorescein were recorded at 30 frames per second in real-time using the camera (Fig. 1c and 1d). The room temperature was kept at 22 °C, and the ambient lighting was maintained dark consistently. The experiments with each test solution were repeated four times for reliable results with less than 5% standard deviation. Unlike the other conventional pH measurement techniques, this set up did not require the conventional pH probe, creating an undisturbed environment for testing (Marinenko et al., 1986; Monteiro et al., 2021). Additionally, this set up enables spatially and temporally resolved pH measurements in 1D allowing us to track dynamic pH change throughout the microchannel at 5 µm and 10 ms, respectively.

2.4. Image processing

Information on real-time changes in fluorescein's emission intensity along the channel was extracted from the recorded experimental video in MATLAB. It should be noted that the changes in emission intensity perpendicular to the channel were negligible and hence, averaged out for simplification in further analysis. Intensity changes along the channel were then mapped onto a calibration curve relating intensity to pH, providing the corresponding pH changes.

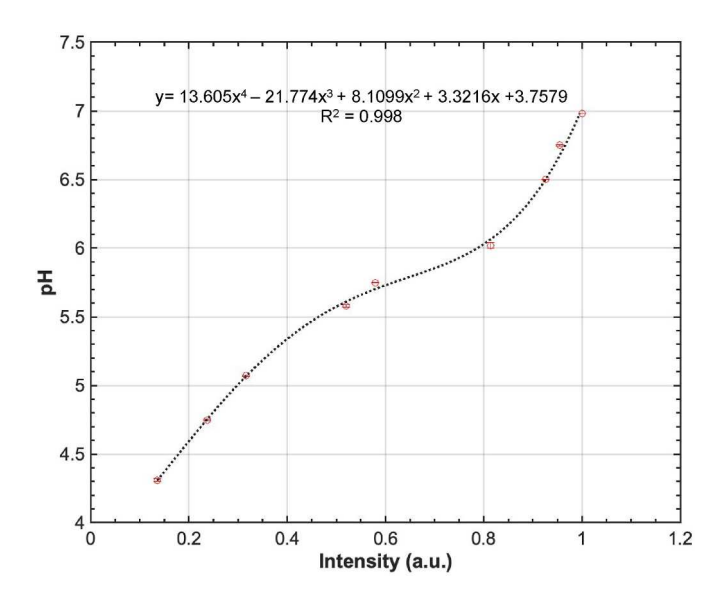


Fig. 2. Calibration curve of pH as a function of fluorescein's emission intensity fitted to a 4th-degree polynomial function along with error bars. The error bars are invisible because of the small values.

2.5. Electrolysis for CO2 storage

Electrolysis was needed to study the seawater-concrete solution for CO_2 storage. This process invokes drastic changes in local pH near the electrodes to drive precipitation. A conventional electrolysis H-cell was used and filled with solution. A platinum-coated titanium electrode was placed on each side of the H-cell. The DC power supply then provided power at 30 V and 6 amps for 5 min. To evaluate the electrolysis performance, the solution pH was measured before and after the electrolysis using the portable pH probe.

2.6. Raman spectroscopy and electron microscopy

The precipitates from electrolysis experiments were analyzed by Raman spectroscopy as follows. The precipitates were transferred to centrifuge tubes and isolated by centrifugation at 4000g for 5 min. Supernatants were discarded, and the precipitates were washed five times with HPLC-grade water with repeated centrifuging. The washed precipitates were transferred to a CaF2 microscope slide and dried under vacuum at 30 °C overnight. Raman spectra were collected from the dried samples using a HORIBA XploRA ONE Raman microscope (532 nm laser, 10x objective, 2400 g/mm grating, 100 μm hole, 50 μm slit). Spectra from reagent grade CaCO3 and MgCO3 were collected in the same manner for comparison. Scanning electron microscopy (SEM) was performed on precipitates using a Coxem EM-30N microscope. For scanning transmission electron microscopy (STEM) and energy dispersive spectroscopy (EDS), precipitates were placed on formvar-coated copper grids and analyzed by a 120 kV JEOL JM-1400 transmission electron microscope in a beryllium sample holder.

3. Results and discussion

3.1. pH calibration of fluorescein

For the calibration of pH changes to fluorescein's emission intensity, nine different buffer solutions were prepared using a mixture of potassium dihydrogen phosphate (KH_2PO_4) and sodium hydroxide (NaOH). These buffers had pH values ranging from about 4 to 7, within the pH sensitivity of fluorescein between 3.5 and 7 (Diehl and Markuszewski, 1989). With a 200 μ M concentration of fluorescein, the intensity values of all the solutions were measured and subsequently plotted against pH.

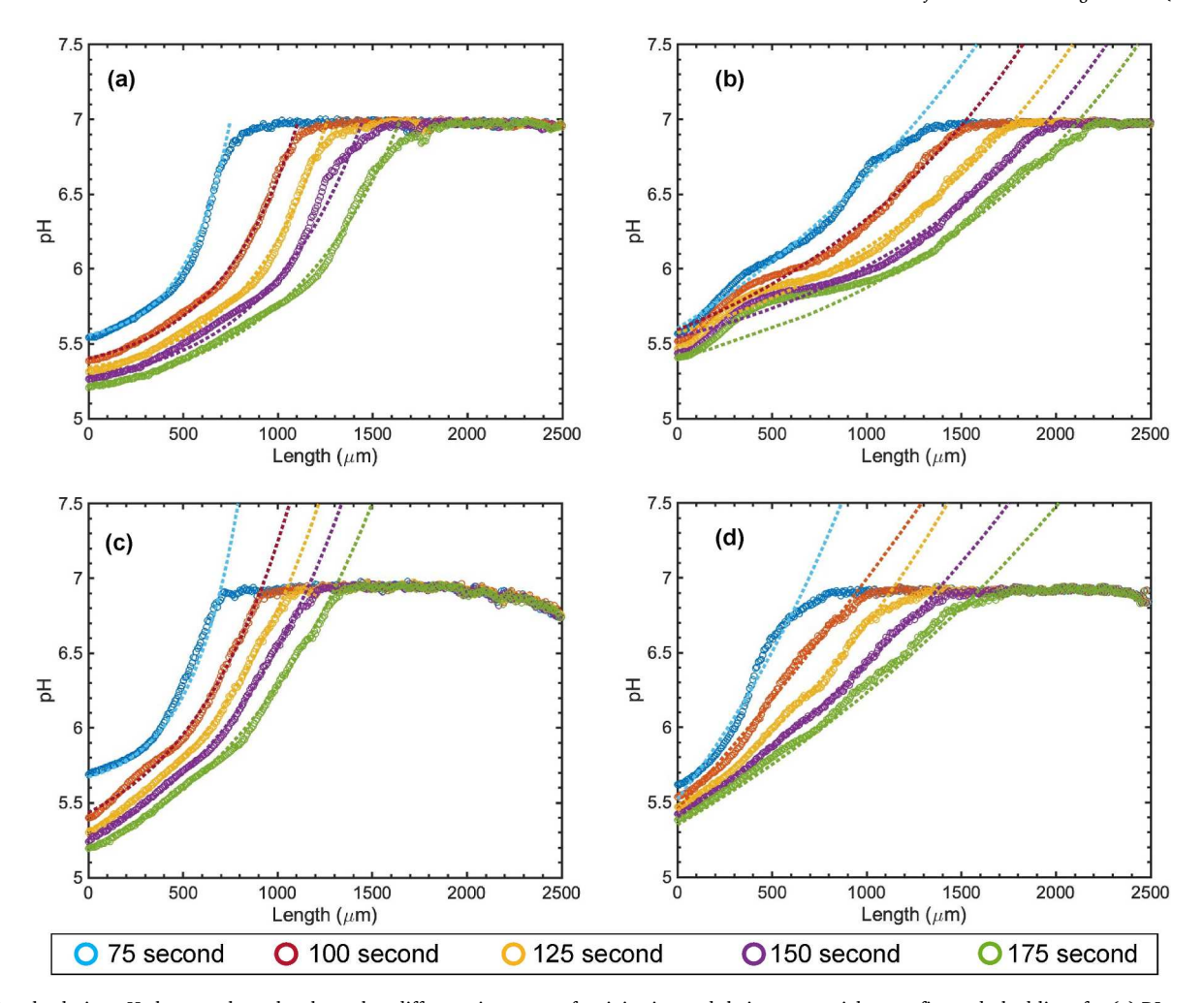


Fig. 3. Local solution pH changes along the channel at different time steps after injection and their exponential curve fits as dashed lines for (a) DI water, (b) DI water-concrete, (c) Seawater, and (d) Seawater-concrete solutions.

Fig. 2 shows the calibration results with a polynomial curve fitting the measured data with $R^2 = 0.998$. The maximum relative standard deviation of the pH measurements was 1.5%.

3.2. CO₂ dissolution analysis

The CO_2 dissolution and its rate can be estimated by the time-dependent change of solution pH caused by CO_2 absorption. The absorption of gaseous CO_2 in an aqueous solution is diffusion-driven (when there is no convective flow) and governed by Henry's law (eq (1)), where K_H represents Henry's constant, which is used to find the theoretical CO_2 solubility in a given solution. Upon absorption, CO_2 reacts with water to form carbonic acid, which deprotonates into bicarbonate and carbonate ions while producing H^+ ions, decreasing pH (eqs (2)–(4)).

$$CO_{2(g)} \xrightarrow{K_H} CO_{2(gg)} \tag{1}$$

$$CO_{2(aq)} + H_2O \xrightarrow{K_c} H_2CO_{3(aq)}$$
 (2)

$$H_2CO_{3(aq)} \xrightarrow{K_1} H^+ + HCO_{3(aq)}^-$$
 (3)

$$HCO_{3(qa)}^{-} \stackrel{K_2}{\to} H^+ + CO_{3(qa)}^{2-}$$
 (4)

Here, K_C , K_1 , and K_2 denote equilibrium constants in each reaction, which can be calculated with empirical models (Millero et al., 2007).

Fig. 3 shows the time-dependent pH changes along the channel for four test solutions at time steps of 75, 100, 125, 150, and 175 s after the gas-fluid interface (i.e., meniscus) was formed. Each dataset at a given time step was averaged with four experimental results. The typical error of these results is negligible (for example, the maximum error is 0.1% in DI water). Since the pH sensitivity of fluorescein is limited to a maximum of 7, the measured pH asymptotes at 7 in all the solutions, regardless of initial pH. In all experiments, the lower pH is observed closer to the meniscus (0 μ m) due to the more prolonged exposure to CO2. The pH values increase with different gradual slopes along the channel according to the inherent CO2 dissolution characteristic in each test solution. It should be noted that the time-dependent changes of pH values with different slopes at different times provide different degrees of CO₂ dissolution rates. At 175 s after CO₂ injection, a variation of solution pH was observed at 1800 ± 25 and 1320 ± 25 μm in the DI water (Fig. 3a) and seawater (Fig. 3c), respectively. In comparison, pH variances were observed at 2150 \pm 25 μm and 1730 \pm 25 μm for DI water-concrete (Fig. 3b) and seawater-concrete (Fig. 3d), respectively. The shorter distance from the meniscus to the intact solution at pH 7 (i. e., where no observable pH change has occurred) indicates that the ${\rm CO_2}$ dissolution occurs more slowly due to the lower dissolution rate or diffusion rate, therefore transferring CO2 molecules less effectively from the meniscus toward the solution inlet (Fig. 1c). This behavior is more noticeable in seawater-based solutions (Fig. 3c and d) than in DI-water-based ones (Fig. 3a and b).

Inherently low dissolution of CO₂ in seawater is well documented, attributed to salinity effects (i.e., increased salinity contributing to a

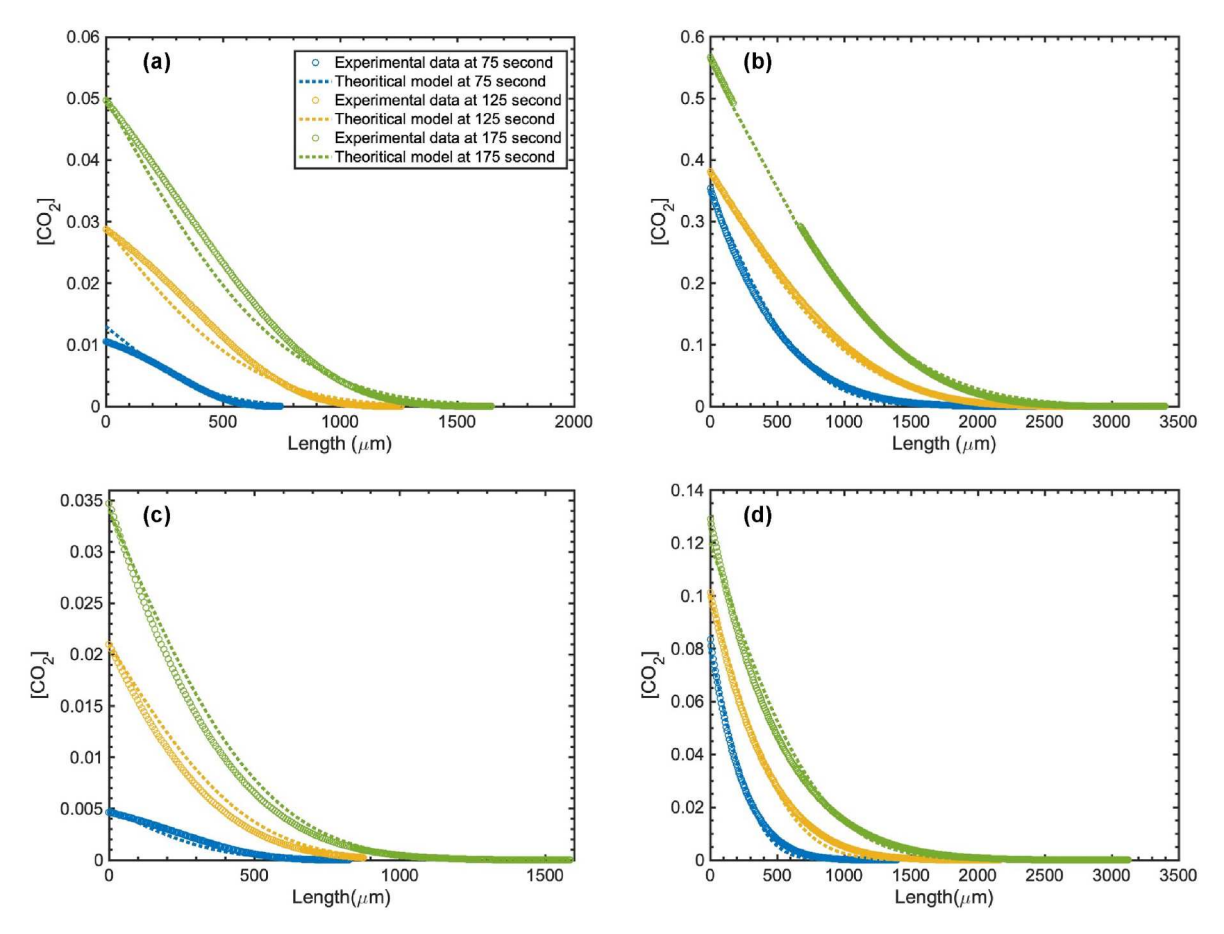


Fig. 4. Estimated CO₂ concentrations along the channel (symbols) and the diffusion models (dotted lines) at different time steps in (a) DI water, (b) DI water-concrete, (c) Seawater, and (d) Seawater-concrete solutions.

reduction in CO_2 dissolution) (Seo et al., 2020). However, the results suggest that adding waste concrete increases CO_2 dissolution significantly in both seawater and DI water, increasing CO_2 absorption, which is seen in the distances where the pH values vary. This phenomenon is because CO_2 is dissolved more actively in an alkaline solution. When concrete is added to an aqueous solution, calcium oxide (i.e., lime) in concrete is dissociated, increasing pH and Ca^{2+} concentration and making the solution alkaline, which are favorable conditions for CO_2 dissolution (Seinfeld and Pandis, 2008). The pH of DI water was measured, increasing from 7 to 10, while the seawater pH increased from 7.8 to 9.5 by adding 10 g/L concrete.

By comparing the pH variation of the solvent, we found that the seawater-concrete solution performs lower than pure DI water (i.e., 1730 µm in seawater-concrete in Fig. 3d vs. 1800 µm in DI water in Fig. 3a) even after the concrete had been added. This behavior is due to the inability to measure the change in fluorescein's emission intensity at basic pH. The initial pH of seawater, seawater-concrete, and DI waterconcrete solutions were all greater than 7, impossible to be measured by fluorescein. To estimate the pH change greater than 7 based on the measured data, we used an extrapolation method, providing a curve fit for the pH-distance relationship using exponential and polynomial functions. Exponential functions were found to be the best representation of the data with R^2 values closest to 1 and were used to extrapolate pH values beyond 7 (Supporting Information). It should be noted that the results with exponential functions provide conservative estimations; for example, in DI water (Fig. 3a), the distance from the meniscus to the location with pH 7 is much shorter in calculation with exponential functions than observation from the experiments. Additionally, diffusion is typically modeled with exponential functions (Chen et al., 2017). With the extrapolation, the distance of pH variations can be approximated as

 $1746~\mu m$ and $1611~\mu m$ in DI water and seawater, respectively, at 175~s. Similarly, with the addition of concrete, the pH variation reaches $3398~\mu m$ and $3123~\mu m$ in DI water-concrete and seawater-concrete solutions, respectively. This suggests that the seawater-concrete solution would perform better for CO_2 dissolution than pure DI water.

To estimate the amount of dissolved CO2 in the solvent (i.e., solubility) from pH measurements, we considered the speciation of dissolved CO_2 in an aqueous solution using eqs (1)–(4). Here, we develop a model for CO2 dissolution based solely on pH change under current experimental conditions (see SI for details). A more comprehensive model would be required to accurately predict CO2 dissolution if the concrete contains major amounts of CO₂ dissolution hindering compositions, like salt. The concentration of total dissolved CO₂ (TDC) at time t, [CO₂ (TDC)]t, is equal to the sum of all possible "forms" of CO2 and is expressed in eq (5). With the assumption of rapid equilibrium, the equilibrium constants in eqs (2)–(4) can be expressed as shown in eq (6) (Mitchell et al., 2010). To determine the concentration of carbonic acid at any given time t, we formulated eq (7) (Supporting Information), where the subscript 0 represents the values at t = 0 while the subscript t represents the values at t. At some time after CO₂ exposure, the change in [H⁺] and [OH⁻] represents the amount of [H⁺] generated from CO₂ dissolution over that time. Using eqs (6) and (7), the concentration of carbonic acid can be expressed in eq (8) at time t, which can be determined from the pH measurement.

$$[CO_{2(TDC)}]_{t} = [CO_{2(aq)}]_{t} + [H_{2}CO_{3}]_{t} + [HCO_{3}^{-}] + [CO_{3}^{2-}]$$
(5)

$$K_{C} = \frac{[H_{2}CO_{3}]_{t}}{[CO_{2(aq)}]_{t}} K_{1} = \frac{[H^{+}]_{t}[HCO_{3}^{-}]_{t}}{[H_{2}CO_{3}]_{t}} K_{2} = \frac{[H^{+}]_{t}[CO_{3}^{2-}]_{t}}{[HCO_{3}^{-}]_{t}}$$
(6)

$$[H^{+}]_{0} - [OH^{-}]_{0} = [H^{+}]_{1} - [OH^{-}]_{1} - [HCO_{3}^{-}]_{1} - 2[CO_{3}^{2-}]_{1}$$
(7)

$$[H_2CO_{3(aq)}] = \frac{[H^+]_t^3 - K_w[H^+]_t + [OH^-]_0 - [H^+]_0)[H^+]_t^2}{K_1([H^+]_t + 2K_2)}$$
(8)

To determine TDC at any given time t, we combined eqs (5) and (6) to get eq (9). This equation shows that measurements of initial pH, real-time pH, and empirical equilibrium constants can provide the estimation of temporal changes in TDC. With eq (9), the change in TDC can be estimated from the change in pH and equilibrium constants.

$$[CO_{2(TDC)}]_t = [H_2CO_3]_t \left[1 + \frac{1}{K_c} + \frac{K_1}{[H^+]_c} + \frac{K_1K_2}{[H^+]_c}\right]$$
 (9)

Fig. 4 displays temporal changes in CO₂ concentration according to the distance along the microchannel at three different time steps at 75, 125, and 175 s. The CO₂ concentration was estimated using eq (9), based on the pH regression data in Fig. 3. In all test solutions at different time steps, the CO₂ concentration decreases exponentially along the channel and reaches zero, where no CO2 dissolution occurred. In addition, the CO₂ concentration increases at the same location with time as CO₂ dissolves. For example, TDC is 0.010, 0.028, and 0.049 M at the meniscus at 75, 125, and 175 s in DI water. On the other hand, at a given time step, TDC differs at the same channel location in different solutions. The pH change after 150 s is negligible in all the test solutions and started to saturate from the meniscus. At 175 s, the estimated CO2 concentrations at the meniscus are 0.049M (2.14 g/L) and 0.0347 M (1.49 g/L) in DI water and seawater, respectively. These concentrations increase to 0.57 M (25.08 g/L) and 0.129 M (5.72 g/L) in DI waterconcrete and seawater-concrete, respectively. These values represent the solubility of the CO2 in respective solutions. Moreover, these increases indicate that the waste concrete enhances CO2 dissolution in DI water and seawater with 12 times and 4 times increase, respectively, compared to their counterparts without concrete. The CO2 solubility results of the seawater is 0.0347M which is well aligned with Henry's law at near atmospheric value of CO₂ (0.5PSIG) with 0.0007M difference (Li et al., 2018). Many parameters like handling of the sample, calibration, testing instrument's accuracy can be sources of error. In the current approach considering the pH meter accuracy, the error propagation calculations show the error in the experimental results are 3.6 μM (0.007%), 34 μ M (0.1%), 292 μ M (0.05%), 5.2 μ M (0.04%) in DI water, seawater, DI water-concrete and seawater-concrete, respectively. Based on the previously published article, the average CO2 dissolution and total alkalinity measurement reports are 0.5 to 0.1% accurate (Bockmon and Dickson, 2015). In comparison to the report analytics, this method yields better results.

In addition to the CO₂ solubility, the rate of CO₂ dissolution into the test solutions was estimated. The gas dissolution into a solution is generally governed by diffusive and convective mass transport (LIU et al., 2016; Seager et al., 2018; Wang et al., 2020). In our experiments, convective effects are negligible as no macroscopic mass transport occurred while temperature and pressure are maintained constant. It is clear in the literature that the diffusion coefficient of CO2 gas in an aqueous solution is directly proportional to its dissolution rate when there is no convective motion of the fluid (Cho and Choi, 2019). Therefore, a semi-infinite, one-dimensional diffusion model, called Fick's law of diffusion (Chen et al., 2017; Crank, 1979; Sell et al., 2013) (eq (12)), was used to find the diffusion coefficient and to study the effect of concrete on dissolution rate. To obtain the diffusion coefficient, the plots of CO₂ concentration in Fig. 4 were fitted to Fick's diffusion model where the gas-liquid interface is considered the highest concentration of CO_2 (c_0). Here, D represents the diffusion coefficient (µm (A Pielkejr et al., 2005)/s), x is the distance in the direction of diffusion (μm) , and t represents the time (s).

$$c = c_0 erfc\left(\frac{x}{\sqrt{4Dt}}\right) \tag{12}$$

 Table 1

 Estimated diffusion coefficients for different test solutions.

Solution	D (μm (A Pielkejr et al., 2005)/s)
DI water	800
DI water with concrete	2600
Seawater	530
Seawater with concrete	835

The dotted lines in Fig. 4 show the diffusion models, fitted to eq (12), for the four test solutions at 75, 125 and 175s after the meniscus is formed. Fig. 4 shows that the experimental results align well with the theoretical models. Using these models associated with eq (12), we estimated the diffusion coefficient D, as shown in Table 1. It should be noted that, although diffusion models are shown in Fig. 4 at three-time steps for better visibility, D in Table 1 represents the average value with five-time steps. Based on diffusion coefficients in Table 1, it can be estimated that the rate of dissolution in seawater (530 μ m²/s) is lower than that of DI water (800 μ m²/s), corresponding to our observations of CO₂ solubility in Fig. 3. As aforementioned, the strong ionic activity of the salt in seawater hinders CO₂ dissolution. However, the diffusion coefficient of seawater improves by 57.54%, surpassing that of the DI water despite salinity effects, with the addition of 10 g/L concrete.

The DI water-concrete solution had an average diffusion coefficient of 2600 µm²/s, the highest among all test solutions in this study. It should be noted that the CO2 concentration data near the meniscus does not completely align with the theoretical model. This discrepancy is probably attributed to calcium carbonate precipitation observed in the microchannel, which was most likely driven by the high pH. The high alkalinity promotes the formation of carbonate ions (CO_2^{2-}) , which combine with calcium ions (Ca^{2+}). This precipitate was redissolved as CO2 invokes acidity, buffering pH change (Fig. 3b and Supporting Information). The seawater-concrete solution also contains ample amounts of calcium ions, but precipitation was not observed in the microchannel. This is likely due to a lower pH than the DI waterconcrete solution and the presence of other dications (i.e., Mg²⁺) and organic compounds, which may slow precipitation (Moras et al., 2022). Nonetheless, as discussed in Section 3.3, the potential to store CO₂ in the form of solid calcium carbonate still exists in seawater-concrete solutions with proper modifications of fluid properties.

3.3. CO₂ storage analysis

One critical benefit of seawater-concrete-based CO₂ capture is the high possibility of creating biologically benign carbonate minerals simultaneously from the associated CO2-water reactions, which are an important building block for many sea creatures, such as shells and coral reefs. In the ocean, precipitation naturally occurs, forming various minerals (Coggon et al., 2012). However, under a test environment, mineral precipitation was not observed in the seawater-concrete solution, although substantial amounts of alkaline dications are available. This is because of the absence of bio-organisms that incite precipitation and atmospheric temperature (Turchyn et al., 2021). An increase in the temperature of the seawater-concrete solutions may drive precipitation (Riding, 1992), but this process could be very energy-demanding, especially at a large commercial scale. As an alternative, we propose to use electrolysis to drive carbonate precipitation, although further studies on costs/benefits comparing lowering temperatures to electrolysis are required to determine the most practical approach on a commercial scale. Since seawater is an electrically conductive solution, electrolysis can be directly performed without any additional conductive agents. Additionally, seawater electrolysis produces industrially sought-after gases (i.e., hydrogen, chlorine, and oxygen) as byproducts. There have been many studies published in a similar field (Xia et al., 2023; Yan et al., 2022). Electrolysis drives the precipitation of alkaline carbonate minerals (carbon storage) by drastic shifts in the protonation

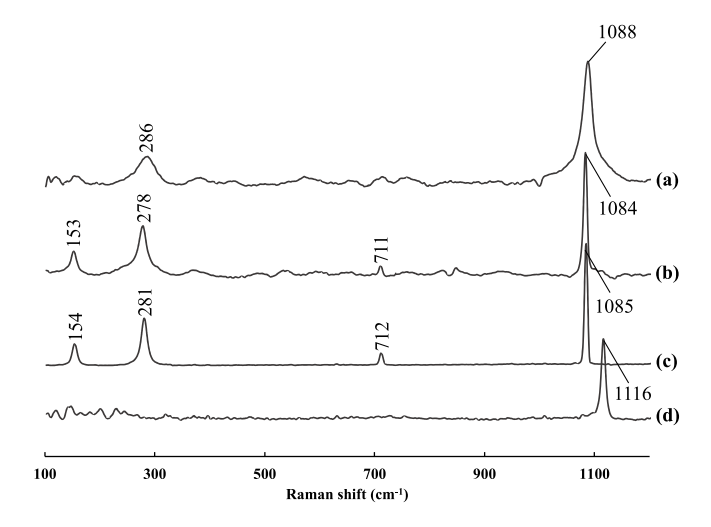


Fig. 5. Raman Spectra of (a) Seawater-concrete precipitates, (b) DI water-concrete precipitates, (c) Pure CaCO₃, and (d) Pure MgCO₃.

states, and hence equilibriums of carbonate species. Upon electrolysis the local pH nearthe cathode increases substantially,causing the overwhelming majority of carbonic acid and bicarbonate ions to dissociate forming carbonate ions (Cosmo et al., 2023). These carbonate ions may then precipitate with alkaline ions into alkaline carbonate minerals.

Electrolysis was performed in the same seawater-concrete solutions used for CO_2 capture and storage. After 5 min of electrolysis, the local pH near the cathode increased to 12, and we found that this was sufficient for considerable precipitation to occur. To analyze the precipitated minerals, Raman spectroscopy was performed. Raman spectra of precipitates indicated that both DI water-concrete and seawater-concrete solutions yielded calcium carbonate (Fig. 5).

The presence of distinct lattice vibrational bands at 152 and 279 ${\rm cm}^{-1}$ in the Raman spectrum of the DI water-concrete precipitate suggests calcite formation. A lack of lattice vibrational bands and a

broadened internal vibrational band at 1080 cm⁻¹ in the spectrum of the seawater-concrete precipitate indicate an amorphous calcium carbonate (Wang et al., 2012). Electron microscopy was used to further analyze the structure of the precipitates. SEM images showed a more ordered structure for the precipitate from DI water-concrete solutions compared to seawater-concrete solutions (Fig. 6). This confirms the observation from Raman spectra that precipitation in seawater-concrete was likely to be amorphous. The presence of numerous ionic species, particularly magnesium, in the seawater-concrete solution, is likely responsible for the amorphous state of seawater-concrete precipitates (Wang et al., 2012). It should be noted that this amorphous state of CaCO3 is more useful in the growth of aqua health (i.e., corals, crustaceans, etc.) (Mass et al., 2017). The precipitates were analyzed by MP-OES, and to our surprise the seawater-concrete precipitate contained more magnesium than calcium (Supporting Information). This was confirmed by scanning transmission electron microscopy (TEM) paired with energy-dispersive spectroscopy (STEM-EDS) which showed precipitates dominated by magnesium signals (Fig. 6e). The strong presence of magnesium in the seawater-concrete precipitate is likely a result of its greater concentration in the seawater-concrete solution (Supporting Information) and its theoretically more rapidly forming hydrated carbonate complexes than calcium (Hu et al., 2020).

4. Conclusion

Freshwater-amine solutions have shown excellent CO_2 dissolution in commercial power plants. However, the scarcity of freshwater, toxicity of amine chemicals, and cost- and energy-intensive operations deem water-amine unreasonable for large-scale applications. As a more sustainable option, this study shows that waste concrete-seawater could be a potentially effective solvent for CO_2 capture and storage, which can possibly be used in industries as an environmentally green solution. The waste concrete raises the solution pH (from 7.8 to 9.5) and alkalinity in seawater solutions. With the addition of concrete, the maximum TDC estimated from the change in pH is increased by a factor of 12 and 4, and dissolution rates increase by 225% and 57.54% in DI water and seawater, respectively. In addition, the seawater-concrete solution was

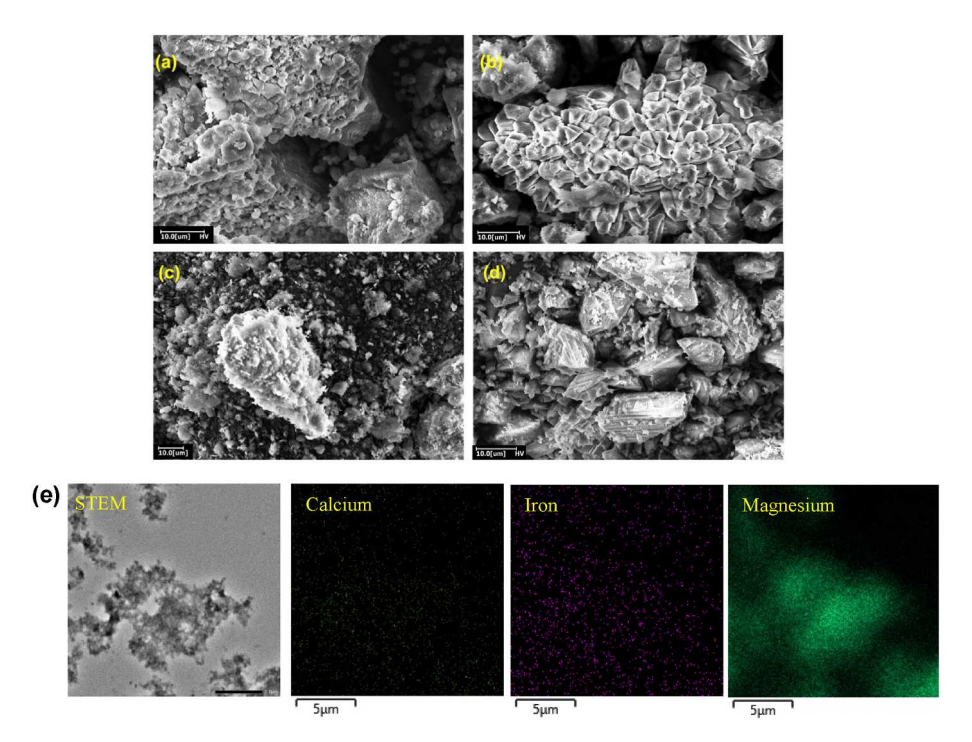


Fig. 6. SEM images of (a) Seawater-concrete precipitates, (b) DI water-concrete precipitates, (c) Pure MgCO₃, and (d) Pure CaCO₃. The scale bar represents 10 μm. (e) TEM image with STEM-EDS analysis for seawater-concrete precipitates.

subjected to electrolysis following the controlled contact with $\rm CO_2$ to favor the precipitation of carbonates as an alternative storage option. Raman spectra and SEM analyses determine seawater electrolysis yields amorphous calcium and magnesium carbonates, effectively storing the captured carbon. The highest $\rm CO_2$ dissolution of the proposed study is around 5.72 g/L, which is significantly lower than the conventional methods like amine scrubbing (more than 100 g/L with similar physical parameters to this study) (Jou et al., 1995). However, this method could be viable if other parameters like regeneration, cost of solvent, in-situ storage, and environmental impact are considered. Before speculating the proposed method's implementation into existing industrial $\rm CO_2$ capture and storage technologies, a thorough cost benefit analysis is required. Additionally, to verify the performance of the proposed solution on an industrial scale, a large-scale experimental analysis will be the focus of future work.

Author statement

Abhishek Ratanpara: Conceptualization, Methodology, Software, Data Curation, Formal analysis, Writing - Original Draft, Writing - Review & Editing Supervision, Project administration John G. Ricca: Methodology, Software, Investigation, Validation, Formal analysis, Writing - Original Draft, Writing - Review & Editing Ayush Gowda: Investigation, Software, Writing - Original Draft, Abel Abraham: Investigation, Data Curation, Writing - Original Draft, Sofia Wiskoff: Investigation, Visualization, Writing - Original Draft, Victor Zauder: Data Curation, Writing - Original Draft Ria Sharma: Investigation, Writing - Original Draft, Meeongsub Kim: Conceptualization, Resources, Writing - Original Draft, Writing - Review & Editing, Supervision, Project administration.

Disclosure statement from the U.S. Geological Survey

The views and conclusions contained in this document are those of the authors and should not be interpreted as representing the opinions or policies of the U.S. Geological Survey. Mention of trade names or commercial products does not constitute their endorsement by the U.S. Geological Survey.

Declaration of competing interest

The authors declare the following financial interests/personal relationships which may be considered as potential competing interests: Myeongsub Kim reports financial support was provided by National Science Foundation. Abhishek Ratanpara reports financial support was provided by National Science Foundation. John G. Ricca reports financial support was provided by US Geological Survey. Myeongsub Kim reports financial support was provided by Florida Center for Environmental Studies.

Data availability

Data will be made available on request.

Acknowledgments

This work was financially supported by the Janke Research Fund from the Center for Environmental Studies at Florida Atlantic University, National Science Foundation (award #: 2207642), and the U.S. Geological Survey (Grant #: G18AC00311). The financial support from the FAU's Office of Undergraduate Research and Inquiry is also greatly acknowledged. We thank Dr. Bobby Duersch for his assistance with SEM and TEM.

Appendix A. Supplementary Data

Supplementary data to this article can be found online at https://doi.org/10.1016/j.jenvman.2023.118760.

References

- A Pielkejr, B R; Landsea, C.; Mayfield, M.; Layer, J.; Pasch, R. Hurricanes and Global Warming. 2005, https://doi.org/10.1175/BAMS-86-II-1571..
- Baena-Moreno, F.M., Leventaki, E., Riddell, A., Wojtasz-Mucha, J., Bernin, D., 2022. Effluents and residues from industrial sites for carbon dioxide capture: a Review. Environ. Chem. Lett. 21 (1), 319–337. https://doi.org/10.1007/S10311-022-01513-x
- Bennaceur, K., Gupta, N., Monea, M., Ramakrishnan, J.S., Randen, T., Sakurai, S., Whittaker, S., 2004. CO_2 capture and storage a solution within. Oilfield Rev. 16, 44–61.
- Bockmon, E.E., Dickson, A.G., 2015. An inter-laboratory comparison assessing the quality of seawater carbon dioxide measurements. Mar. Chem. 171, 36–43. https:// doi.org/10.1016/j.marchem.2015.02.002.
- Botha, A., Strydom, C.A., 2001. Preparation of a Magnesium Hydroxy Carbonate from Magnesium Hydroxide. www.elsevier.com/locate/hydromet.
- Chen, Y., Wang, J., Flanagan, D.R., 2017. Chapter 9 fundamental of diffusion and dissolution. In: Qiu, Y., Chen, Y., Zhang, G.G.Z., Yu, L., Mantri, R. v (Eds.), Developing Solid Oral Dosage Forms, second ed. Academic Press, Boston, pp. 253–270. https://doi.org/10.1016/B978-0-12-802447-8.00009-1.
- Cho, H.J., Choi, J., 2019. Calculation of the mass transfer coefficient for the dissolution of multiple carbon dioxide bubbles in sea water under varying conditions. J. Mar. Sci. Eng. 7 (12) https://doi.org/10.3390/JMSE7120457.
- Coggon, R.M., Teagle, D.A., Harris, M., John, C.M., Smith-Duque, C.E., Alt, J., Coggon, R. M., Teagle, D.A., Harris, M., John, C.M., Smith-Duque, C.E., Alt, J., 2012. Why does calcium carbonate precipitate in the ocean crust? Am. Geophys. Union Fall Meet. 2012. B33D-0545.
- Cosmo, R. de P., Rinaldi, R., Pereira, F. de A.R., Soares, E.J., Martins, A.L., 2023. CO₂ degassing in CaCO₃ precipitation in the presence of oil: implications, modeling, numerical simulation, validation, prototype development, and experimental results. Geoenergy Sci. Eng. 228, 211885 https://doi.org/10.1016/J.GEOEN.2023.211885.
- Crank, J., 1979. The Mathematics of Diffusion. Oxford university press.
- Diehl, H., Markuszewski, R., 1989. Studies on fluorescein—VII: the fluorescencGeoenergy Sci. Eng.e of fluorescein as a function of PH. Talanta 36 (3), 416–418. https://doi.org/10.1016/0039-9140(89)80213-9.
- Gagg, C.R., 2014. Cement and concrete as an engineering material: an historic appraisal and case study analysis. Eng. Fail. Anal. 40, 114–140. https://doi.org/10.1016/j. engfailanal.2014.02.004.
- Hu, Y., Vasiliu, M., Thanthiriwatte, K.S., Jackson, V.E., Chaka, A.M., Dixon, D.A., 2020. Thermodynamics of metal carbonates and bicarbonates and their hydrates for Mg, Ca, Fe, and Cd relevant to mineral energetics. J. Phys. Chem. A 124 (9), 1829–1840. https://doi.org/10.1021/acs.jpca.9b11741.
- Jou, F.-Y., Mather, A.E., Otto, F.D., 1995. The solubility of CO₂ in a 30 mass percent monoethanolamine solution. Can. J. Chem. Eng. 73 (1), 140–147. https://doi.org/ 10.1002/CJCF.5450730116.
- Jung, J., Jeong, Y.S., Lim, Y., Lee, C.S., Han, C., 2013. Advanced CO₂ capture process using MEA scrubbing: configuration of a split flow and phase separation heat exchanger. Energy Proc. 37, 1778–1784. https://doi.org/10.1016/j. egypro.2013.06.054.
- Kazemian, M., Shafei, B., 2023. Carbon sequestration and storage in concrete: a state-of-the-art Review of compositions, methods, and developments. J. CO2 Util. 70, 102443 https://doi.org/10.1016/J.JCOU.2023.102443.
- Li, H., Tang, Z., Xing, X., Guo, D., Cui, L., Mao, X. Zhong, 2018. Study of CO₂ capture by seawater and its reinforcement. Energy 164, 1135–1144. https://doi.org/10.1016/J. ENERGY.2018.09.066.
- Liu, Q., Endo, H., Fukuda, K., Shibahara, M., Zhang, P., 2016. Experimental study on solution and diffusion process of single carbon dioxide bubble in seawater. Mech. Eng. J. 3 (5) https://doi.org/10.1299/mej.16-00269, 16-00269-16-00269.
- Lv, B., Guo, B., Zhou, Z., Jing, G., 2015. Mechanisms of CO₂ capture into monoethanolamine solution with different CO₂ loading during the absorption/ desorption processes. Environ. Sci. Technol. 49 (17), 10728–10735. https://doi.org/ 10.1021/acs.est.5b02356.
- Ma, J., Li, L., Wang, H., Du, Y., Ma, J., Zhang, X., Wang, Z., 2022. Carbon Capture and Storage: History and the Road Ahead. Engineering. Elsevier Ltd July 1, pp. 33–43. https://doi.org/10.1016/j.eng.2021.11.024.
- Magneschi, G., Zhang, T., Munson, R., 2017. The impact of CO₂ capture on water requirements of power plants. Energy Proc. 114, 6337–6347. https://doi.org/ 10.1016/j.egypro.2017.03.1770.
- Marinenko, G., Paule, R.C., Koch, W.F., Knoerdel, M., 1986. Effect of variables on PH measurement in acid-rain-like solutions as determined by ruggedness tests. J. Res. Natl. Bur. Stand. 91 (1), 17. https://doi.org/10.6028/JRES.091.004 (1934).
- Mass, T., Giuffre, A.J., Sun, C.Y., Stifler, C.A., Frazier, M.J., Neder, M., Tamura, N., Stan, C.v., Marcus, M.A., Gilbert, P.U.P.A., 2017. Amorphous calcium carbonate particles form coral skeletons. Proc. Natl. Acad. Sci. U. S. A. 114 (37), E7670–E7678. https://doi.org/10.1073/PNAS.1707890114.
- Millero, F., Huang, F., Graham, T., Pierrot, D., 2007. The dissociation of carbonic acid in NaCl solutions as a function of concentration and temperature. Geochimica et Cosmochima Acta 71 (1), 46–55. https://doi.org/10.1016/j.gca.2006.08.041.

- Mitchell, M.J., Jensen, O.E., Cliffe, K.A., Maroto-Valer, M.M., 2010. A model of carbon dioxide dissolution and mineral carbonation kinetics. Proc. R. Soc. A 466 (2117), 1265–1290. https://doi.org/10.1098/rspa.2009.0349.
- Monteiro, M.C.O., Mirabal, A., Jacobse, L., Doblhoff-Dier, K., Barton, S.C., Koper, M.T. M., 2021. Time-resolved local PH measurements during CO2Reduction using scanning electrochemical microscopy: buffering and tip effects. JACS Au 1 (11), 1915–1924. https://doi.org/10.1021/JACSAU.1C00289/ASSET/IMAGES/MEDIUM/AU1C00289 M018.GIF.
- Moras, C.A., Bach, L.T., Cyronak, T., Joannes-Boyau, R., Schulz, K.G., 2022. Ocean alkalinity enhancement - avoiding runaway CaCO₃ precipitation during quick and hydrated lime dissolution. Biogeosciences 19 (15), 3537–3557. https://doi.org/ 10.5194/bg-19-3537-2022.
- Nayak, N.C., Yue, C.Y., Lam, Y.C., Tan, Y.L., 2010. Thermal bonding of PMMA: effect of polymer molecular weight. Microsyst. Technol. 16 (3), 487–491. https://doi.org/ 10.1007/S00542-009-0926-Y/FIGURES/6.
- Nayak, N., Mehrotra, R., Mehrotra, S., 2022. Carbon bio sequestration strategies: a Review. Carbon Capture Sci. Technol. 4, 100065 https://doi.org/10.1016/J. CCST.2022.100065.
- Ratanpara, A.P., Shaw, A., Deshpande, S., Kim, M., 2020. Utilization of ocean water for CO₂ capture via amine scrubbing. In: Proceedings of the International Conference on Offshore Mechanics and Arctic Engineering OMAE, 5. https://doi.org/10.1115/OMAE.2020.10315
- Ratanpara, A., Shaw, A., Thomas, M., Patel, R.N., Kim, M., 2021. Microfluidic analysis of seawater-based CO_2 capture in an amine solution with nickel nanoparticle catalysts. J. CO2 Util. 53, 101712 https://doi.org/10.1016/j.jcou.2021.101712.
- Riding, R., 1992. Temporal variation in calcification in marine cyanobacteria. J. Geol. Soc. (Lond.) 149 (6), 979–989. https://doi.org/10.1144/GSJGS.149.6.0979.
- Ringrose, P.S., Furre, A.-K., Gilfillan, S. M. v, Krevor, S., Landrø, M., Leslie, R., Meckel, T., Nazarian, B., Zahid, A., 2021. Storage of carbon dioxide in saline aquifers: physicochemical processes, key constraints, and scale-up potential. Annu. Rev. Chem. Biomol. Eng. 12 (1), 471–494. https://doi.org/10.1146/annurevchembioeng-093020-091447.
- Ritchie, H.; Spooner, F.; Roser, M. Biodiversity. Our World in Data. https://doi.org/10.1 073/PNAS.1711842115..

- Sabine, C.L., Feely, R.A., Gruber, N., Key, R.M., Lee, K., Bullister, J.L., Wanninkhof, R., Wong, C.S., Wallace, D.W.R., Tilbrook, B., Millero, F.J., Peng, T.H., Kozyr, A., Ono, T., Rios, A.F., 2004. The oceanic sink for anthropogenic CO₂. Science 305 (5682), 367–371. https://doi.org/10.1126/science.1097403.
- Seager, R.J., Acevedo, A.J., Spill, F., Zaman, M.H., 2018. Solid dissolution in a fluid solvent is characterized by the interplay of surface area-dependent diffusion and physical fragmentation. Sci. Rep. 8 (1), 7711. https://doi.org/10.1038/s41598-018-25891.
- Seinfeld, J., Pandis, S., 2008. Atmospheric Chemistry and Physics, from Air Pollution to Climate Change, 1997. New York.
- Sell, A., Fadaei, H., Kim, M., Sinton, D., 2013. Measurement of CO₂ diffusivity for carbon sequestration: a microfluidic approach for reservoir-specific analysis. Environ. Sci. Technol. 47 (1), 71–78. https://doi.org/10.1021/es303319q.
- Seo, S., Lages, B., Kim, M., 2020. Catalytic CO₂ absorption in an amine solvent using nickel nanoparticles for post-combustion carbon capture. J. CO2 Util. 36, 244–252. https://doi.org/10.1016/J.JCOU.2019.11.011.
- Skocek, J., Zajac, M., ben Haha, M., 2020. Carbon capture and utilization by mineralization of cement pastes derived from recycled concrete. Sci. Rep. 10 (1) https://doi.org/10.1038/s41598-020-62503-z.
- Turchyn, A.v., Bradbury, H.J., Walker, K., Sun, X., 2021. Controls on the precipitation of carbonate minerals within marine sediments. Front. Earth Sci. 9, 57. https://doi.org/ 10.3389/FEART.2021.618311/BIBTEX.
- Wang, D., Hamm, L.M., Bodnar, R.J., Dove, P.M., 2012. Raman spectroscopic characterization of the magnesium content in amorphous calcium carbonates. J. Raman Spectrosc. 43 (4), 543–548. https://doi.org/10.1002/JRS.3057.
- Wang, L., Huang, X., Wang, D., 2020. Solubility and diffusion coefficient of supercritical CO₂ in polystyrene dynamic melt. E-Polymers 20 (1), 659–672. https://doi.org/
- Xia, Q., Zhang, K., Zheng, T., An, L., Xia, C., Zhang, X., 2023. Integration of CO₂ capture and electrochemical conversion. ACS Energy Lett. 8 (6), 2840–2857. https://doi. org/10.1021/ACSENERGYLETT.3C00738/ASSET/IMAGES/LARGE/NZ3C00738_ 0009.JPEG.
- Yan, L., Bao, J., Shao, Y., Wang, W., 2022. An Electrochemical Hydrogen-Looping System for Low-Cost CO₂ Capture from Seawater. https://doi.org/10.1021/ acsenergylett.2c00396.